Electrically controlled nuclear polarization of individual atoms

Kai Yang [1], Philip Willke [1,2,3], Yujeong Bae [1,2,3], Alejandro Ferrón[4], Jose L. Lado[5,6], Arzhang Ardavan [7], Joaquín Fernández-Rossier[5,8], Andreas J. Heinrich[2,3]* and Christopher P. Lutz [1]*

Nuclear spins serve as sensitive probes in chemistry[1] and materials science[2] and are promising candidates for quantum information processing[3-6]. NMR, the resonant control of nuclear spins, is a powerful tool for probing local magnetic environments in condensed matter systems, which range from magnetic ordering in high-temperature superconductors[7,8] and spin liquids[9] to quantum magnetism in nanomagnets[10,11]. Increasing the sensitivity of NMR to the single-atom scale is challenging as it requires a strong polarization of nuclear spins, well in excess of the low polarizations obtained at thermal equilibrium, as well as driving and detecting them individually[4,5,12]. Strong nuclear spin polarization, known as hyperpolarization, can be achieved through hyperfine coupling with electron spins[2]. The fundamental mechanism is the conservation of angular momentum: an electron spin flips and a nuclear spin flops. The nuclear hyperpolarization enables applications such as in vivo magnetic resonance imaging using nanoparticles[13], and is harnessed for spin-based quantum information processing in quantum dots[14] and doped silicon[15-17]. Here we polarize the nuclear spins of individual copper atoms on a surface using a spin-polarized current in a scanning tunnelling microscope. By employing the electron–nuclear flip-flop hyperfine interaction, the spin angular momentum is transferred from tunnelling electrons to the nucleus of individual Cu atoms. The direction and magnitude of the nuclear polarization is controlled by the direction and amplitude of the current. The nuclear polarization permits the detection of the NMR of individual Cu atoms, which is used to sense the local magnetic environment of the Cu electron spin.

The electrical control of nuclear spins can be achieved using alternating[4,6] or static[18] electric fields, as well as electric current[19,20]. Compared to magnetic[5] and optical control[12], electrical control is particularly appealing for applications, because electric fields are relatively easy to generate locally and allow individual spins to be addressed[4]. We used an electric current to control the nuclear magnetism of individual atoms in a scanning tunnelling microscope (STM) (Fig. 1a) and demonstrated the all-electric polarization and resonant driving of the single nuclear spin of a Cu atom. The Cu nuclear spin is polarized with either polarity, by as much as 30%, which is ~17 times greater than thermal polarization at 1 K. This is achieved by employing a spin-transfer torque effect at the single-atom level (Fig. 1b).

The Cu atoms were deposited on a MgO decoupling layer grown on a Ag(001) substrate (Fig. 1a). This set-up makes individual Cu atoms electrically accessible to the probe tip of STM by measuring the time-average d.c. current (I_{DC})[21]. Each Cu atom adsorbs on top of the oxygen site (Supplementary Fig. 1a) and has an electron spin $S=1/2$, as determined below. Cu occurs naturally in two stable isotopes[22]: ^{63}Cu (~69%) and ^{65}Cu (~31%), and both have a nuclear spin $I=3/2$. We modelled the coupled electron–nuclear system of Cu ($S=1/2$, $I=3/2$) in a magnetic field **B** by using an isotropic hyperfine coupling term and electron Zeeman term:

$$H = A\mathbf{S} \cdot \mathbf{I} + \gamma_e \mathbf{B} \cdot \mathbf{S} \qquad (1)$$

Here A is the hyperfine constant and γ_e is the electron gyromagnetic ratio. The anisotropic components of the hyperfine coupling and electric quadrupole coupling are much weaker (<100 MHz according to the density functional theory (DFT) calculations in Supplementary Section 1), and are omitted here, as is the nuclear Zeeman energy.

We probed the quantum states of individual Cu atom by using inelastic electron tunnelling spectroscopy[23] and electron spin resonance (ESR)[24–26]. Inelastic electron tunnelling spectroscopy reveals spin excitations between the states with electron spin quantum number $m_S=\pm1/2$ (labelled as ↑ and ↓), by measuring the differential conductance (dI/dV) spectra (Fig. 2a). By fitting the electron Zeeman splitting as a function of the B field (Fig. 2a, inset)[27], we obtained an electron g factor of 1.98 ± 0.10 and $\gamma_e=g\mu_B/h=27.7\pm1.4\,\mathrm{GHz\,T^{-1}}$ (h is Planck's constant and μ_B is the Bohr magneton). This suggests that Cu has an electron spin $S=1/2$, as confirmed by our DFT calculations.

We resolved the hyperfine structure[26] of individual Cu atoms by driving ESR transitions between the ↑ and ↓ states using a spin-polarized tip (Supplementary Fig. 3) with an energy resolution of ~100 neV. The four ESR peaks (Fig. 2b) correspond to the four different orientations of the nuclear spin $I=3/2$ (Fig. 2d). The hyperfine constant A can be extracted from the four ESR frequencies, $A=(f_{II}+f_{IV}-f_I-f_{III})/2$ (Supplementary Sec. 5). The histogram of the A values (Fig. 2b, right inset) shows two separate Gaussian peaks at 2.86 ± 0.03 and $3.05\pm0.07\,\mathrm{GHz}$, which correspond to the two isotopes ^{63}Cu and ^{65}Cu, respectively. This demonstrates the capability of ESR–STM to distinguish different isotopes with atomic precision, even when the nuclear spin magnitude is equal.

[1]IBM Almaden Research Center, San Jose, CA, USA. [2]Center for Quantum Nanoscience, Institute for Basic Science (IBS), Seoul, Republic of Korea. [3]Department of Physics, Ewha Womans University, Seoul, Republic of Korea. [4]Instituto de Modelado e Innovación Tecnológica (CONICET-UNNE) and Facultad de Ciencias Exactas, Naturales y Agrimensura, Universidad Nacional del Nordeste, Corrientes, Argentina. [5]QuantaLab, International Iberian Nanotechnology Laboratory (INL), Braga, Portugal. [6]Institute for Theoretical Physics, ETH Zurich, Zurich, Switzerland. [7]Clarendon Laboratory, Department of Physics, University of Oxford, Oxford, UK. [8]Departamento de Física Aplicada, Universidad de Alicante, San Vicente del Raspeig, Spain. *e-mail: heinrich.andreas@qns.science; cplutz@us.ibm.com
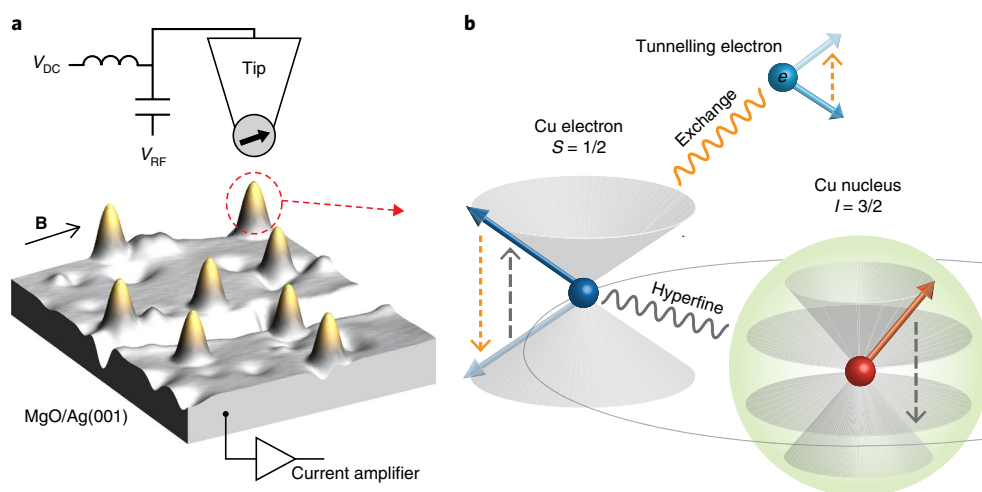
Fig. 1 | Electrical polarization of the nuclear spin of a Cu atom on MgO. a, Schematic of the experimental set-up that consists of an STM with an ESR capability, and an STM image of Cu atoms (yellow protrusions) on a MgO bilayer on Ag(001) (set point: $V_{DC} = 50\,mV$, $I_{DC} = 20\,pA$). An in-plane magnetic field (**B**) is applied to set the electron Zeeman energy of Cu. Both V_{DC} and radiofrequency (V_{RF}) voltages are applied to the STM junction to perform ESR. The tip apex is labelled by a black arrow to indicate that the tip is spin polarized. **b**, Mechanism of the nuclear spin polarization for the coupled electron ($S = 1/2$) and nuclear ($I = 3/2$) spin system. The tunnelling electron changes the orientation of the Cu electron spin (dashed orange arrows) by an exchange interaction (orange wavy line), and angular momentum is subsequently transferred from the Cu electron to the Cu nucleus (dashed grey arrows) by the flip-flop hyperfine interaction (grey wavy line).

The hyperfine constant is sensitive to the chemical environment of an atom[26,28], here the bonding configuration of Cu on MgO. DFT calculations revealed that the electron spin occupies mainly (~60%) the 4s orbital (Fig. 2b, left inset). The large hyperfine constant of Cu on MgO, compared to that in other environments[28], thus arises from the large s electron density at the nucleus, which yields an unusually large Fermi contact interaction[2]. The calculated hyperfine constants ($A = 3.76$ and $4.02\,GHz$ for ^{63}Cu and ^{65}Cu, respectively) agree well with the experimental values.

We plot the energy diagram of a Cu atom in Fig. 2c. The eight eigenstates are labelled as $|i\rangle$ ($i = 1$ to 8). In the limit of a high B field (electron Zeeman energy much larger than that of hyperfine coupling), the eigenstates are nearly the Zeeman product states $|m_S, m_I\rangle$, where $m_S = \uparrow, \downarrow$ and $m_I = \pm 3/2, \pm 1/2$. In general, the state $|\downarrow, m_I\rangle$ hybridizes with $|\uparrow, m_I - 1\rangle$ ($m_I = +3/2, \pm 1/2$) due to the flip-flop hyperfine interaction (S^+I^- and S^-I^+), to form three pairs of hybrid states ($|i\rangle$ and $|8-i\rangle$ with $i = 1, 2$ and 3) (ref. [3]). For example, at $B = 0.65\,T$, the Zeeman energy is about six times larger than the hyperfine coupling for both isotopes, and states $|\downarrow, +3/2\rangle$ and $|\uparrow, +1/2\rangle$ mix to form $|1\rangle \approx 0.99|\downarrow, +3/2\rangle - 0.12|\uparrow, +1/2\rangle$ and $|7\rangle \approx 0.12|\downarrow, +3/2\rangle + 0.99|\uparrow, +1/2\rangle$. Owing to the slight overlap between eigenstates $|i\rangle$ and $|8-i\rangle$ ($|\langle i |S_z| 8-i\rangle|^2 \neq 0$), tunnelling electrons can induce state transitions by scattering with the Cu electron, during which the spin of the tunnelling electron is conserved ($\Delta\sigma = 0$). In comparison, $\Delta\sigma = \pm 1$ transitions (tunnelling electron reverses its spin) can occur between $|i\rangle$ and $|9-i\rangle$ because $|\langle i |S_x| 9-i\rangle|^2 \neq 0$ (x indicates a direction perpendicular to the spin quantization axis z). We use these two types of current-induced transitions to control the nuclear polarization, as shown below.

The nuclear polarization, $P_n = \langle I_z \rangle / I$ (z indicates the quantization axis of the nuclear spin), is only ~1.7% for ^{63}Cu or ^{65}Cu at thermal equilibrium ($B = 0.65\,T$, $T = 1.2\,K$). This polarization results from the Boltzmann occupation of nuclear substates separated by only ~$A/2$. The main thermal relaxation path is probably through the scattering by electrons from the Ag substrate[21,29].

We controlled P_n using a spin-polarized current that flows through an individual Cu atom, with the readout of P_n simultaneously realized by taking ESR spectra. Note that the ESR-induced transition rate is much smaller than the current-induced rates

(Supplementary Fig. 5) and thus the ESR process only weakly perturbs P_n. Figure 3a,b shows the ESR spectra taken with spin-polarized currents of opposite directions given by opposite bias polarities. The relative amplitudes of the ESR peaks directly reveal the steady-state populations of each nuclear spin state at a large I_{DC}. We found that a sufficiently large negative bias (electrons tunnel from sample to tip), and thus large current when holding the tip height constant, led to nuclear spin polarization primarily into the $m_I = -3/2$ states (Fig. 3a). Reversing the current direction by applying a positive bias led to a higher occupation of the $m_I = +3/2$ states (Fig. 3b). Figure 3c shows the ESR amplitudes as a function of sample d.c. bias at a constant tip height. Increasing the d.c. voltage (V_{DC}) and thus I_{DC} increases the degree of nuclear polarization, which saturates to a limiting polarization at large I_{DC}.

The current-controlled nuclear polarization is a consequence of the conservation of total spin angular momentum through two spin-transfer torque processes at the single-atom level (Fig. 1b). The principle is illustrated in Fig. 3d,e for each bias polarity. For example, at a positive V_{DC}, tunnelling electrons first exchange spin angular momentum with the localized Cu electron spin by exchange scattering (blue arrow in the upper panel of Fig. 3e). This spin-reversing ($\Delta\sigma = -1$) electron tunnelling pumps the electron spin of the Cu atom from the four lower states to the upper states ($\Delta m_S = +1$) to conserve angular momentum[29]. At a large I_{DC}, the population ratio between the two states with the same m_I (between $|i\rangle$ and $|9-i\rangle$) is set by the spin polarization (η) of the tip to give a ratio of $(1+\eta)/(1-\eta)$, where $\eta \approx 0.19$ for this tip (from the fit in Fig. 3c). The second step of the spin-transfer torque occurs between the nuclear and electron spins of the Cu atom via the flip-flop hyperfine interaction. At a large I_{DC}, this process is mainly driven by the spin-conserving ($\Delta\sigma = 0$) electron tunnelling events (dashed grey arrows in Fig. 3e), which equalize the populations of the connected states ($|i\rangle$ and $|8-i\rangle$). At a low I_{DC}, the scattering of electrons from the Ag substrate sets the Boltzmann distribution of the connected states.

Considering all the transitions, the state population at a positive V_{DC} follows the paths indicated by the arrows in Fig. 3e, and the net effect is that the nuclear spin is driven towards the states $|1\rangle$ and $|8\rangle$, which are mainly composed of $m_I = +3/2$, which gives a positive P_n.
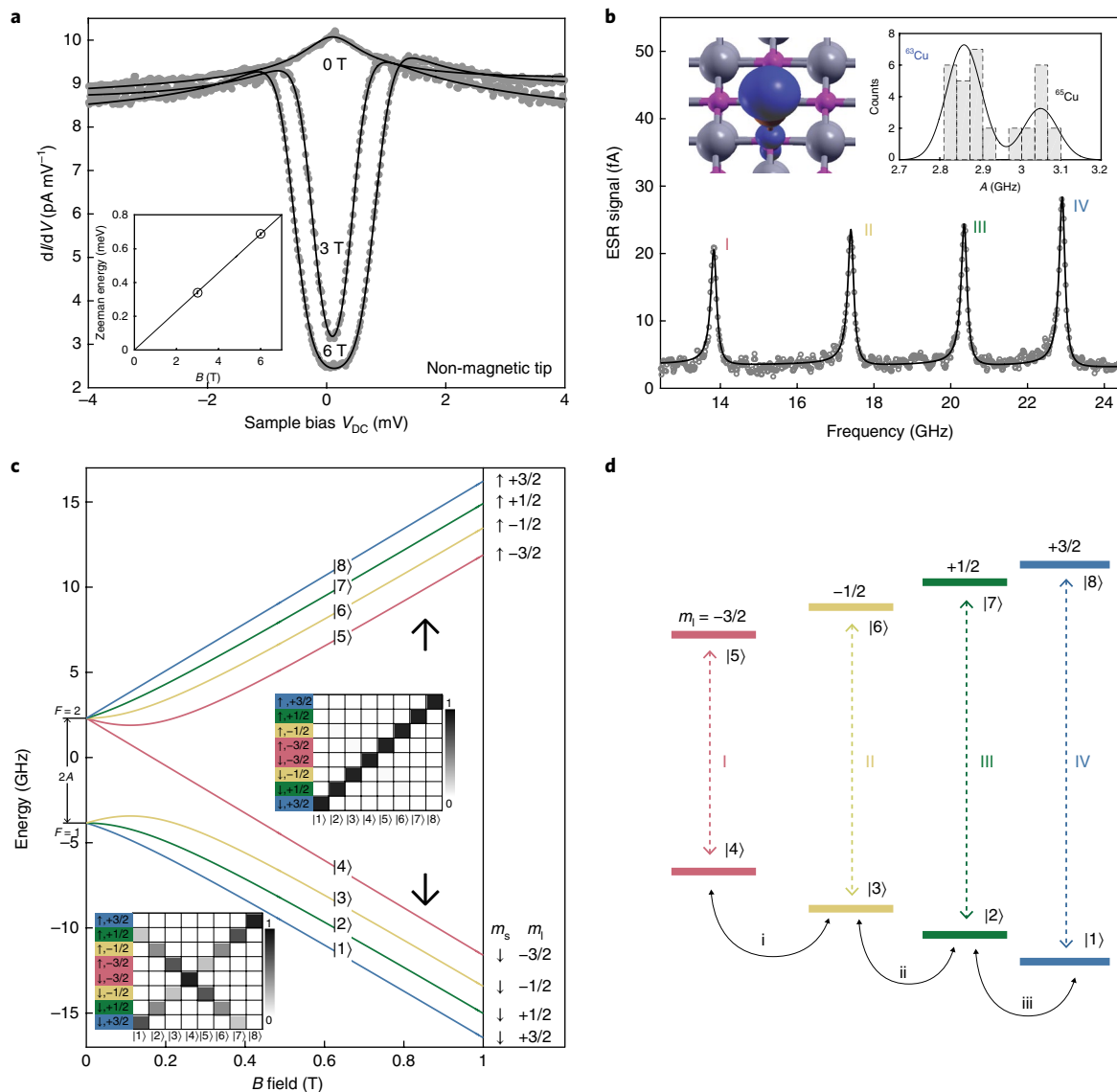
Fig. 2 | Electronic and hyperfine structures of a single Cu atom on MgO. a, dI/dV spectra of Cu at different magnetic fields (0 T, 3 T and 6 T) with a non-magnetic tip (set point: $V_{DC} = 10$ mV, $I_{DC} = 100$ pA, $T = 0.6$ K). The spectra are vertically shifted for clarity. The position of the conductance steps reveals the Zeeman energy. The zero-bias peak at zero field is a Kondo resonance (Supplementary Fig. 2). Inset: magnetic field dependence of the Zeeman energy. A linear fit constrained to zero Zeeman energy at zero field yields a g factor of 1.98 ± 0.10. **b**, ESR spectrum of a ^{65}Cu atom with four peaks labelled as I–IV (set point: $V_{DC} = -20$ mV, $I_{DC} = 40$ pA, $V_{RF} = 15$ mV, total field $B = 0.65$ T (consists of an external field of 0.765 T and an effective tip field), $T = 1.2$ K). Left inset: calculated spin density (dark blue) of Cu on MgO. Right inset: histogram of the hyperfine constant A of 31 Cu atoms, fitted by two Gaussians. The ratio of 0.93 ± 0.02 between the two mean values at the Gaussian peaks agrees well with the ratio (0.9336) between the hyperfine constants of ^{63}Cu and ^{65}Cu measured by the atomic beam technique[22]. **c**, Energy diagram of the electron–nuclear spin system as a function of the B field ($S = 1/2$, $I = 3/2$). Insets: schematic of the energy eigenstates, labelled as $|i\rangle$ ($i = 1$ to 8) of the Hamiltonian in equation (1), at $B = 0$ (bottom) and 0.65 T (top). Each column represents one eigenstate. The grey level represents the probability amplitudes in the basis of Zeeman product states $|m_S, m_I\rangle = |m_S\rangle \otimes |m_I\rangle$, where the electron and nuclear spin quantum numbers are $m_S = \uparrow, \downarrow$ and $m_I = \pm 3/2, \pm 1/2$, respectively. At zero field, the eight eigenstates consist of a triplet (total spin $F = 1$) and a quintet ($F = 2$). At 0.65 T, the eight eigenstates are nearly Zeeman product states (Supplementary equation (3)). Note that states $|\downarrow, -3/2\rangle$ ($|4\rangle$) and $|\uparrow, +3/2\rangle$ ($|8\rangle$) are exact eigenstates for all values of the B field. **d**, Schematic energy level diagram at 0.65 T showing ESR transitions (vertical arrows) and NMR transitions (arc arrows), labelled by I–IV and i–iii, respectively.

Similarly, at a negative sample bias, the populations are driven to $m_I = -3/2$ states (Fig. 3d), to give a negative P_n.

To quantitatively describe the behaviour of the electron and nuclear spin of Cu under the influence of the spin-polarized current, we developed a rate equation model (Supplementary Section 6). This model considers the transition rates between states due to the scattering with electrons that tunnel between the tip and Ag, as well as the scattering by Ag substrate electrons (which originate

from Ag and return to Ag), using a quantum mechanical transition intensity operator[29]. By fitting the ESR amplitudes versus V_{DC} in Fig. 3c to our model, we obtained P_n at different V_{DC} (Fig. 3f, solid curve). At a large current, P_n can be approximated directly from the ratios of the four ESR amplitudes at each V_{DC} (dashed curve in Fig. 3f). The ESR amplitudes (Fig. 3c) and the corresponding calculated P_n (Fig. 3f, dashed curve) show an asymmetry with respect to the zero bias, due to the different spin pumping directions at opposite bias
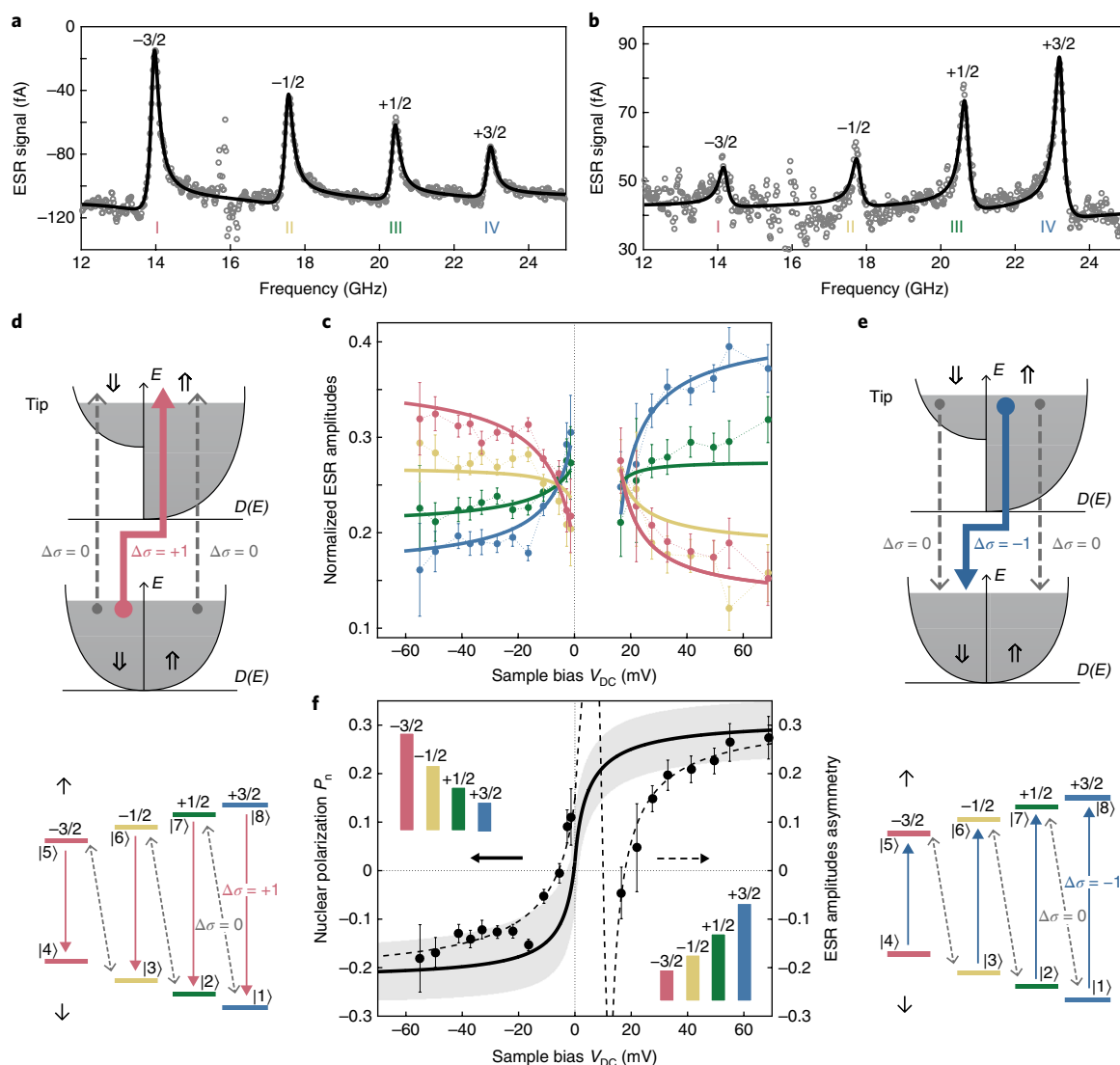
Fig. 3 | Spin-transfer torque of the Cu nuclear spin. a,b, ESR spectra of a ^{65}Cu atom at $V_{DC} = -22$ mV (**a**) and $+22$ mV (**b**) for the same tip (set point: $I_{DC} = 60$ pA, $V_{RF} = 12$ mV, total field $B = 0.66$ T consisting of an external field of 0.74 T and an effective tip field; $T = 1.2$ K). The four peaks correspond to four nuclear spin states ($m_I = \pm 3/2, \pm 1/2$). **c**, Normalized ESR amplitudes as a function of sample bias measured with a different tip than that in **a** and **b** (set point: $V_{DC} = 22$ mV, $I_{DC} = 80$ pA, $V_{RF} = 6-20$ mV, $B = 0.66$ T, $T = 1.2$ K). Negative (left) and positive (right) sides are fitted separately using the rate equation model (Supplementary equation (15)), to give a tip polarization η of 0.14 (0.19) at a negative (positive) bias. Error bars are determined by the fitting uncertainties of the ESR peak amplitudes at each V_{DC}. **d**, Mechanism of the nuclear polarization at negative bias. Upper panel: $\Delta\sigma = +1$ (red arrow) and $\Delta\sigma = 0$ (dashed grey arrows) electron tunnelling between the spin-dependent ($\Uparrow$ or $\Downarrow$) densities of states $D(E)$ of Ag and the STM tip. Lower panel: $\Delta\sigma = +1$ tunnelling drives the Cu electron spin from $m_s = \uparrow$ to $\downarrow$ (red arrows); $\Delta\sigma = 0$ tunnelling drives the flip-flop transitions (dashed grey arrows) between the nuclear spin states labelled by $m_I = \pm 3/2, \pm 1/2$. The magnetic tip here is anti-aligned with the ground-state Cu electron spin. Oppositely aligned tip torques the nuclear spin in the opposite directions (Supplementary Fig. 3). The weaker tunnelling process with the opposite spin-flip sign ($\Delta\sigma = -1$) is also present (not pictured). **e**, Mechanism of the nuclear polarization at a positive bias. The weaker tunnelling process ($\Delta\sigma = +1$) is also present (not pictured). **f**, Nuclear polarization P_n as a function of V_{DC} (solid curve) based on fitting the results in **c** using the rate equation model. The uncertainty of P_n is depicted as the shaded region by considering the uncertainties of the fitting parameters with a 95% confidence. The dashed curve is the asymmetry in ESR peak amplitudes calculated from the same model (Supplementary equation (17)). The asymmetry approaches P_n in the limit of a large bias, but deviates from the true nuclear polarization at a small current. Data points are the measured asymmetry obtained directly by weighting the four ESR amplitudes of the same V_{DC} in **c**. The error bars are propagated from the fitting uncertainties of the ESR peak amplitudes at each V_{DC}. Insets: populations of four nuclear spin states at both bias polarities.

polarities. At a positive V_{DC}, thermal relaxation due to the substrate electrons and $\Delta\sigma = -1$ processes due to the spin-polarized tunnel current compete with each other, whereas at a negative V_{DC} both the thermal relaxation and $\Delta\sigma = +1$ processes favour the occupation of the lower-energy states.

The model shows that P_n grows monotonically with V_{DC} and the polarization direction is controlled by the bias polarity. The result

is a fast electrical initialization of the nuclear spin. We found that when the exchange scattering with tunnelling electrons occurs more frequently than the spin relaxation driven by the substrate electrons (every ~10 ns as estimated from the point contact conductance[21]), P_n starts to deviate from the thermal equilibrium. The saturation polarization at $+70$ mV is ~30%, which is a ~17-fold enhancement over the thermal equilibrium. This corresponds to an effective

a

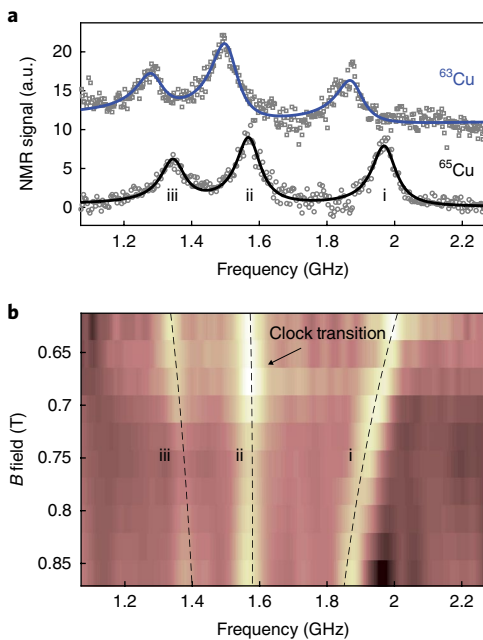**b**

Fig. 4 | NMR-type transitions of single Cu atoms. a, NMR spectra of single ^{63}Cu and ^{65}Cu atoms on MgO (set point: $V_{DC} = -22\,mV$, $I_{DC} = -60\,pA$, $V_{RF} = 25\,mV$, $B = 0.66\,T$, $T = 1.2\,K$). Transitions are labelled as in Fig. 2d, and detected by the change of the magnetoresistance of the electron states using the d.c. current, different to the traditional double resonance technique (Supplementary Fig. 6 gives double resonance spectra)[2]. Transitions between the upper four states ($m_S = \uparrow$) may also contribute to the spectrum, but these should be much weaker owing to their small populations at this spin torque polarity. The solid lines are the fit to three Lorentzian peaks. The spectra are vertically shifted for clarity. **b**, NMR spectra of a ^{65}Cu atom as a function of the total B field (set point: $V_{DC} = 16$–$22\,mV$, $I_{DC} = 60\,pA$). The total B field is varied by changing the tip field at an external field of 0.74 T. The values of the total B field are obtained by measuring the ESR spectra of Cu for each tip position. The dashed lines are the calculated transition frequencies. a.u., arbitrary units.

nuclear spin temperature of ~200 mK, which is six times cooler than the experimental temperature of 1.2 K. The model also shows that the saturation polarization increases monotonically with the tip spin polarization, and reaches unity with a fully polarized tip ($\eta = 1$) (Supplementary Fig. 4). The time needed to reach the steady-state polarization is limited by the rates of the flip-flop transitions ($\Delta\sigma = 0$), which are slower than the $\Delta\sigma = \pm 1$ transitions by a factor of $\alpha = (\gamma_e B/A)^2 \approx 40$. The settling time is thus $\sim 4\alpha(e/I_{DC}) = 420$ ns at an I_{DC} of 60 pA (ref. [29]).

The polarized nuclear spin permits direct access to the resonant transitions between adjacent nuclear spin states ($\Delta m_I = \pm 1$)[2,30] (Fig. 4a). These NMR-type transitions[31] (labelled NMR in the following) are driven by an a.c. voltage applied at the transition frequencies (~$A/2$), and are probably made possible by the mixing of the electron and nuclear states (Supplementary Section 5)[3]. The resonances are detected by the change of electron spin polarization that results from the NMR transitions. The NMR spectrum of single Cu atoms reveals three peaks, which correspond to transitions i–iii labelled in Fig. 2d. The separation of NMR frequencies makes it possible to address each transition individually. The uneven spacing of nuclear states is due to the hyperfine coupling. The relatively broad NMR peaks compared to other nuclear spin systems[4–6] are due to a shorter nuclear coherence time, which is limited by the electron spin relaxation time that results from the interaction with the tunnelling current as well as the scattering electrons from the Ag substrate.

We employed the NMR spectra to probe the local magnetic environment of a ^{65}Cu atom by varying the effective tip magnetic field[25] applied to the atom. The change of the Zeeman energy of the Cu electron spin manifests as an NMR frequency shift (Fig. 4b). Two frequencies (i and iii) shift with the tip magnetic field, whereas the frequency of iii is almost constant at ~1.6 GHz, which agrees well with the calculated evolution (dashed lines in Fig. 4b). The transition ii is an NMR-type clock transition[31,32], a transition that is insensitive to the B field. The clock transition of ^{63}Cu occurs at a smaller frequency of ~1.5 GHz (Fig. 4a) due to its smaller hyperfine constant. The clock transition frequency can thus be used to distinguish two Cu isotopes.

The nuclear spin-transfer torque effect should be applicable to other electron–nuclear quantum devices[3–6], such as the nuclear spins embedded in single-molecule magnets[4]. Although the nuclear spin relaxation time of Cu on MgO is not yet long enough to perform a single-shot readout of the nuclear spin states, it should be possible to improve this by using thicker MgO layers or by using Cu-based molecules[33]. The electrical polarization, driving and detection of the nuclear spin states enable the local spin manipulation for nuclear spintronics[30] and the detection of the atomic-scale magnetic environment in nanomagnets[10,11].

Online content

Any methods, additional references, Nature Research reporting summaries, source data, statements of data availability and associated accession codes are available at https://doi.org/10.1038/s41565-018-0296-7.

References

1. Staudacher, T. et al. Nuclear magnetic resonance spectroscopy on a (5-nanometer)³ sample volume. *Science* **339**, 561–563 (2013).
2. Slichter, C. P. *Principles of Magnetic Resonance* (Springer, Heidelberg, 1996).
3. Morley, G. W. et al. Quantum control of hybrid nuclear–electronic qubits. *Nat. Mater.* **12**, 103–107 (2013).
4. Thiele, S. et al. Electrically driven nuclear spin resonance in single-molecule magnets. *Science* **344**, 1135–1138 (2014).
5. Pla, J. J. et al. High-fidelity readout and control of a nuclear spin qubit in silicon. *Nature* **496**, 334–338 (2013).
6. Sigillito, A. J. et al. All-electric control of donor nuclear spin qubits in silicon. *Nat. Nanotech.* **12**, 958–962 (2017).
7. Alloul, H., Ohno, T. & Mendels, P. ⁸⁹Y NMR evidence for a Fermi-liquid behavior in YBa₂Cu₃O₆₊ₓ. *Phys. Rev. Lett.* **63**, 1700–1703 (1989).
8. Wu, T. et al. Magnetic-field-induced charge-stripe order in the high-temperature superconductor YBa₂Cu₃Oᵧ. *Nature* **477**, 191–194 (2011).
9. Mendels, P. et al. Ga NMR study of the local susceptibility in kagomé-based SrCr₈Ga₄O₁₉: pseudogap and paramagnetic defects. *Phys. Rev. Lett.* **85**, 3496–3499 (2000).
10. Borsa, F., Lascialfari, A. & Furukawa, Y. *Novel NMR and EPR Techniques* (eds Dolinšek, J., Vilfan, M. & Žumer, S.) 297–349 (Springer, Heidelberg, 2006).
11. Micotti, E. et al. Local spin moment distribution in antiferromagnetic molecular rings probed by NMR. *Phys. Rev. Lett.* **97**, 267204 (2006).
12. Dutt, M. V. G. et al. Quantum register based on individual electronic and nuclear spin qubits in diamond. *Science* **316**, 1312–1316 (2007).
13. Cassidy, M. C. et al. In vivo magnetic resonance imaging of hyperpolarized silicon particles. *Nat. Nanotech.* **8**, 363–368 (2013).
14. Urbaszek, B. et al. Nuclear spin physics in quantum dots: an optical investigation. *Rev. Mod. Phys.* **85**, 79–133 (2013).
15. McCamey, D. R., van Tol, J., Morley, G. W. & Boehme, C. Fast nuclear spin hyperpolarization of phosphorus in silicon. *Phys. Rev. Lett.* **102**, 027601 (2009).
16. Simmons, S. et al. Entanglement in a solid-state spin ensemble. *Nature* **470**, 69–72 (2011).
17. Morley, G. W. et al. The initialization and manipulation of quantum information stored in silicon by bismuth dopants. *Nat. Mater.* **9**, 725–729 (2010).
18. Smet, J. H. et al. Gate-voltage control of spin interactions between electrons and nuclei in a semiconductor. *Nature* **415**, 281–286 (2002).
19. Lo, C. C. et al. All-electrical nuclear spin polarization of donors in silicon. *Phys. Rev. Lett.* **110**, 057601 (2013).

20. Trowbridge, C. J. et al. Dynamic nuclear polarization from current-induced electron spin polarization. *Phys. Rev. B* **90**, 085122 (2014).
21. Paul, W. et al. Control of the millisecond spin lifetime of an electrically probed atom. *Nat. Phys.* **13**, 403–407 (2017).
22. Ting, Y. & Lew, H. Hyperfine structure of Cu^{63} and Cu^{65}. *Phys. Rev.* **105**, 581–588 (1957).
23. Heinrich, A. J., Gupta, J. A., Lutz, C. P. & Eigler, D. M. Single-atom spin-flip spectroscopy. *Science* **306**, 466–469 (2004).
24. Baumann, S. et al. Electron paramagnetic resonance of individual atoms on a surface. *Science* **350**, 417–420 (2015).
25. Yang, K. et al. Engineering the eigenstates of coupled spin-1/2 atoms on a surface. *Phys. Rev. Lett.* **119**, 227206 (2017).
26. Willke, P. et al. Hyperfine interaction of individual atoms on a surface. *Science* **362**, 336–339 (2018).
27. Otte, A. F. et al. The role of magnetic anisotropy in the Kondo effect. *Nat. Phys.* **4**, 847–850 (2008).
28. McGarvey, B. R. The isotropic hyperfine interaction. *J. Phys. Chem.* **71**, 51–66 (1967).
29. Loth, S. et al. Controlling the state of quantum spins with electric currents. *Nat. Phys.* **6**, 340–344 (2010).
30. Reimer, J. A. Nuclear hyperpolarization in solids and the prospects for nuclear spintronics. *Solid. State Nucl. Magn. Reson.* **37**, 3–12 (2010).
31. Wolfowicz, G. et al. Atomic clock transitions in silicon-based spin qubits. *Nat. Nanotech.* **8**, 561–564 (2013).
32. Shiddiq, M. et al. Enhancing coherence in molecular spin qubits via atomic clock transitions. *Nature* **531**, 348–351 (2016).
33. Heinrich, B. W., Braun, L., Pascual, J. I. & Franke, K. J. Protection of excited spin states by a superconducting energy gap. *Nat. Phys.* **9**, 765–768 (2013).

Author contributions

K.Y. and C.P.L. designed the experiment. K.Y., P.W. and Y.B. carried out the STM measurements. K.Y. and C.P.L. performed the analysis and developed the rate equation model. A.F., J.L.L. and J.F.-R. performed the DFT calculations. All the authors discussed the results and edited the manuscript.

Competing interests

The authors declare no competing interests.

Additional information

Supplementary information is available for this paper at https://doi.org/10.1038/s41565-018-0296-7.

Reprints and permissions information is available at www.nature.com/reprints.

Correspondence and requests for materials should be addressed to A.J.H. or C.P.L.

Publisher's note: Springer Nature remains neutral with regard to jurisdictional claims in published maps and institutional affiliations.

Methods

Measurements were performed in a homebuilt ultrahigh vacuum ($<10^{-9}$ torr) STM operated at either 0.6 K or 1.2 K, as indicated in the figures. Bilayer MgO was grown on an atomically clean Ag(001) single crystal by thermally evaporating Mg in an O_2 environment[21]. Cu and Fe atoms were deposited in situ from pure metal rods by electron-beam evaporation onto the sample held at ~10 K. An external magnetic field was applied at ~8° off the surface with the in-plane component aligned along the [100] direction of the MgO lattice. STM images were acquired in the constant-current mode and all the voltages refer to the sample voltage with respect to the tip.

The iridium STM tip was coated with silver by indentations into the Ag sample until the tip gave a good lateral resolution in the STM image. To prepare a spin-polarized tip, Fe atoms on MgO were transferred onto the tip by applying voltage pulses (~0.55 V). The degree of spin polarization was verified by the asymmetry in the dI/dV spectra of Cu with respect to voltage polarity.

The ESR (NMR) spectra were acquired by sweeping the frequency of a radiofrequency voltage V_{RF}^{ESR} generated by Agilent E8257D (V_{RF}^{NMR} generated by Tektronix AWG7122C) across the tunnelling junction and monitoring the changes in the tunnelling current. The current signal was modulated at 95 Hz by chopping V_{RF}^{ESR}, which allowed the read out of the current by a lock-in technique[24]. For NMR spectra, V_{RF}^{ESR} was set to 10 GHz (far from any resonance). V_{RF} and V_{DC} voltages were combined at room temperature using a bias tee and an RF diplexer, and applied to the STM tip through a semirigid coaxial cable[24].

Data availability

The data that support the plots within this paper and other findings of this study are available from the corresponding authors upon reasonable request.